Analysis and Characterization of DC Bus Ripple Current of Two-Level Inverters Using The Equivalent Centered Harmonic Approach

Ufuk Ayhan
Student Member, IEEE
Middle East Technical University
Dept. of Electrical and Electronics Engineering
Ankara, 06800, Turkey
ayhanufuk@gmail.com

Ahmet M. Hava
Member, IEEE
Middle East Technical University
Dept. of Electrical and Electronics Engineering
Ankara, 06800, Turkey
hava@eee.metu.edu.tr

***Abstract* - The dc bus PWM ripple current of three-phase two-level voltage source inverters is a function of the PWM method, the load current magnitude, power factor angle, and the modulation index. Thus, the ripple current characteristics are highly involved and difficult to understand. Using the double Fourier integral approach, this paper investigates the ripple current characteristics thoroughly for a wide range of operating conditions and PWM methods. Then, the equivalent harmonic approach is used to lump the ripple current carrier frequency component and its sidebands to the center as a single frequency equivalent (and the same done for the multiples of the carrier). With this approach the capacitor ESR based losses are predicted easily and the dominant frequency range can be understood better. Thus, a better inverter and dc bus capacitor design can be achieved. Analysis is supported by means of simulations and a high degree of correlation is obtained. The paper additionally evaluates and suggests PWM methods for various inverter applications with the dc bus ripple performance being the main constraint. Thus, it is beneficial for the design engineer.**

I. INTRODUCTION

Three-phase Voltage Source Inverters (VSIs) are widely utilized in ac motor drives, uninterruptible power supplies (UPS), renewable energy systems, etc. to control the energy flow precisely, obtain high power quality and high energy efficiency. Pulse Width Modulation (PWM) is the standard approach to operate the inverter switches in order to generate the required output voltages. Due to high frequency switching both the ac and the dc side of the inverter involve high frequency rectangular voltage/current pulses that create stress on the inverter components. This paper studies the dc bus ripple current due to the PWM operation, and it elaborates on the stresses the ripple creates on the dc bus capacitor.

In three-phase inverters, with PWM operation, the inverter input current (dc bus current, I_{dc} in Fig. 1) consists of high frequency rectangular pulses. The average value I_{avg} comes from the supply, while the harmonic content (ripple current) I_{hf} is bypassed through the dc bus capacitor (filter capacitor). The ripple current frequency spectrum is at the carrier frequency (and its sidebands) and its multiples (and their sidebands). The dc bus PWM ripple current and its spectra depend on the modulation index M_i, PWM method, the load (output) current magnitude (I_{om}), and the load power factor angle (φ) (or power factor PF=cos(φ))[1]-[6]. The dc bus current and its spectra influence the inverter design both from the dc bus voltage ripple and dc bus capacitor losses (due to the capacitor equivalent series resistor (ESR) and/or dielectric losses) perspective. Thus, it is important to obtain the detailed dc bus ripple current characteristics for an effective inverter design.

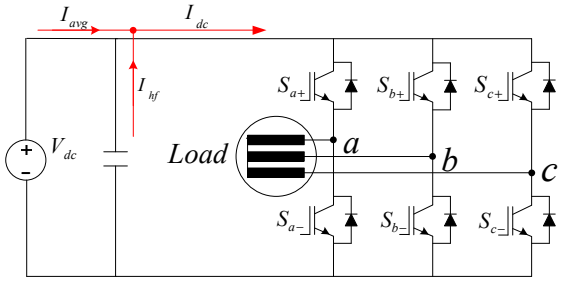

Fig. 1 The dc bus current and its average and ripple components in the three phase two-level inverter topology

Analysis of dc bus current ripple has been previously investigated by means of rms ripple value [1]-[3] and by means of spectral component calculations [4]-[6] for various PWM methods. The rms ripple value obtained via closed form formulas is easy to use, yet it hides the spectral information, which is necessary in analysis and design. The spectral analysis could be conducted by means of detailed computer simulations (labor and computation intensive with case specific results) or by means of analytical methods, for example the double Fourier integral approach (more general, less computations, but requires math skills) [5]-[6]. While literature based on both rms and spectral methods provide various aspects of dc bus current ripple characteristics, comparison based on PWM methods and operating conditions (M_i, φ, I_{om}), understanding of the dominant frequency range in terms of ripple and losses, etc. is lacking.

The prime purpose of the dc bus current ripple analysis is dc bus capacitor design and PWM method selection. However, this analysis by itself is not sufficient to

complete the inverter design process. In various inverter applications, different capacitor types are used and each capacitor technology exhibits different ripple and loss attributes and involves different design rules. Thus, the utilization of the dc bus current ripple and spectrum analysis results requires that the capacitor technology is taken into account. For example, electrolytic and film capacitors have different loss mechanisms and different behavior. Therefore, for each type of application a different capacitor type and different design rules should be considered. For this purpose a basic dc bus capacitor technology classification and design issues should be discussed to guide a proper design. The capacitor suppliers/manufacturers usually provide capacitor operating condition data and give empirical design methods for the design engineer [7]-[13]. There is no clear understanding and a rigorous guide to the inverter design in terms of dc bus capacitor ripple and losses.

Based on the above discussions it becomes obvious, a clear understanding of the dc bus ripple current characteristics and capacitor design study involves very detailed case by case study for each application.

This paper provides an analysis method and graphic tools to overcome these difficulties. In addition to the dc bus current ripple analysis, it also provides a fundamental review of the capacitor technologies which is required in the design. Combining the ripple current analysis and capacitor technology information, then it applies the approach to specific examples to be used in inverter design. It yields the information on correct PWM method and correct capacitor sizing for a given application.

First, a summary of PWM methods will be given. Second, dc bus current ripple of VSI will be inspected; ripple current characteristics depending on the operating point and PWM technique utilized will be studied. The microscopic (per PWM cycle), the rms, and spectral components will be discussed for various PWM method and operating conditions. The double Fourier analysis approach will be briefly reviewed and utilized to generate the spectral data. Then the equivalent centered harmonic approach will be proposed and its results demonstrated. After the introduction of the method, the design stage will be elaborated on. First, the PWM methods in terms of dc bus ripple performance will be compared. Then inverter dc bus capacitor technology will be reviewed and design issues will be discussed. Following the capacitor design examples, the paper will be summed up with conclusion.

II. REVIEW OF PWM METHODS

Among the various PWM methods existing, the following methods are popular due to their simplicity and performance advantages; sinusoidal PWM (SPWM), space vector PWM (SVPWM), discontinuous PWM (DPWM1) [2], active zero state PWM (AZSPWM1) [14], and near state PWM (NSPWM) [15]. The benefits of SPWM and SVPWM are low ripple at low M_i, DPWM1 for low ripple and low loss at high M_i, AZSPWM1 for low common mode voltage and NSPWM for both low common mode voltage and low losses at high M_i[3]. While SPWM, SVPWM and DPWM1 employ a common carrier (triangle), AZSPWM1 and NSPWM employ alternating polarity triangles for each phase [16]. All these methods are easy to implement with modern inverter control chips with advanced PWM generation units. The modulation waves of these methods and the associated carrier signals are shown in Fig. 2.

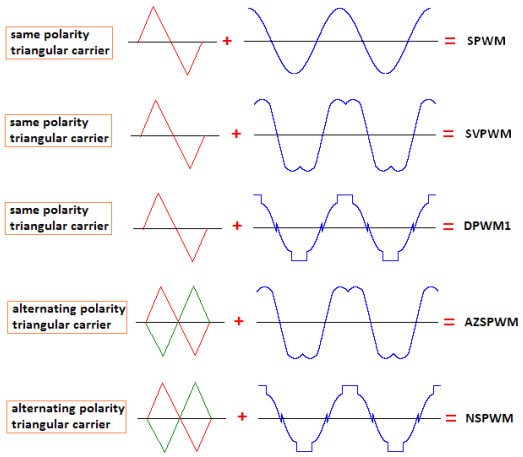

Fig. 2 Two-level three-phase inverter popular PWM methods; the high frequency carrier waves (left) and the modulation waves (right)

III. DC BUS CURRENT RIPPLE OF VSI

This section reviews the dc bus current ripple of the inverter for various operating conditions and PWM methods. The main purpose is to provide a basic tutorial before attempting advanced analysis. First via microscopic waveforms the physical understanding will be established. Second via evaluation of the spectral components the dominant frequency range will be shown. In this section, the spectral data used will be based on the double Fourier approach (also verified by means of computer simulations). Finally the ripple current rms value for various PWM methods will be evaluated for various PWM methods and operating condition.

It is helpful to define a modulation index (M_i, voltage utilization level) term at this stage. For a given dc link voltage (V_{dc}), the ratio of the fundamental component magnitude of the line to neutral inverter output voltage (V_{1m}) to the fundamental component magnitude of the six-step mode voltage ($V_{1m\text{-}6\text{-}step}=2V_{dc}/\pi$) is termed the modulation index M_i [1] as defined in (1).

$$M_i = V_{1m} / V_{1m-6-step} \tag{1}$$

A. Microscopic View

Under sinusoidal steady state operation, the inverter dc bus current ripple instantaneous waveforms appear as picket-fences (as rectangular pulses at the carrier frequency or higher) and their outer appearance depends on the load current magnitude (I_{om}) and power factor, as shown in Fig. 3 (obtained by computer simulations for SVPWM). The magnitude of the sinusoidal load current is the prime factor in determining the magnitude of current pulses. With unity power factor, the current pulses are always with positive value. However, with decreasing power factor negative current pulses appear in the waveform. The average value of the dc bus current

(I_{avg}), is expressed in (2), and it is supplied by the dc voltage source. The difference of I_{dc} and I_{avg} is defined as the ripple current I_h as given in (3), and it is bypassed through the dc bus capacitor.

$$I_{avg} = \left(\frac{3}{\pi}\right) \cdot M_i \cdot I_{om} \cdot \cos\varphi \quad (2)$$

$$I_h = I_{dc} - I_{avg} \quad (3)$$

While Fig. 3 is obtained for SVPWM, it is difficult to distinguish it from the waveforms of other PWM methods by outer appearance. However, as will be shown, in the detailed (microscopic) view, significant differences exist. Thus, the harmonic spectrum of different modulation techniques can be correlated with microscopic analysis of dc bus current within a switching period.

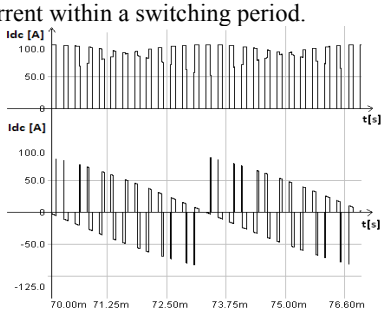

Fig. 3 DC bus current waveform over a 60º of a fundamental cycle for SVPWM under the operating conditions of M_i=0,785, I_{om}=100 A. top: φ = 0°, bottom φ = 90°

As Fig. 4 shows, in SVPWM and AZSPWM1, I_{dc} is composed of two rectangles in a PWM cycle. Thus, they are expected to result in dominant harmonics centered at double the switching frequency ($2f_c$). For φ = 0° the rectangle is full with high average value and low ripple. For φ = 90° the rectangle has low average value and high ripple. Thus, high power factor implies low ripple current. As shown in Fig.5, for DPWM1 and NSPWM, the rectangles are gathered into one piece. Based on the appearance of the waveform shapes, it becomes obvious now strong harmonics exist at both f_c and $2f_c$. For φ = 0° the rectangle is full with high average value and low ripple. For φ increasing the rectangle has low average value and high ripple. Thus, high power factor implies low ripple current. In particular, in NSPWM the φ dependency is strong and the performance rapidly degrades as φ approaches 30°. Apparent from this discussion, the visual observation does not yield sufficient information about the ripple content and spectral analysis is necessary.

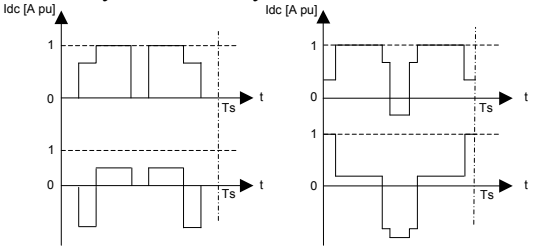

Fig. 4. Inverter microscopic dc bus currents in a PWM period for continuous PWM methods; Left: SVPWM (M_i=0.7, top: φ = 0°, bottom φ = 90°), Right: AZSPWM1 (M_i=0.7, top: φ = 0°, bottom φ = 90°)

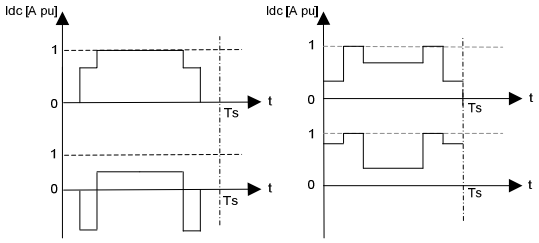

Fig. 5. Inverter microscopic dc bus currents in a PWM period for discontinuous PWM methods; Left: DPWM1 (M_i=0.7, top: φ = 0°, bottom φ = 90°), Right: NSPWM (M_i=0.7, top: φ = 0°, bottom φ = 30°)

B. *Spectral Content*

As apparent from the preceding section, the spectral content of the dc bus ripple current is PWM method dependent, as well as the operating conditions. To illustrate typical spectral content, several methods and operating conditions are considered. A three-phase inverter drive is considered. Balanced sinusoidal operation is assumed. The load current ripple is neglected. The discussed PWM methods with a pure-sinusoidal, 100A peak value rated output current, with 50Hz fundamental frequency are considered. The inverter DC bus is 800V and the carrier frequency (f_c) is 10kHz for SVPWM and AZSPWM1 and 15kHz for NSPWM and DPWM1 such that the average switching frequency is the same (10kHz) in all cases.

The harmonic spectrum for various methods is shown from Fig. 6 to Fig. 11 for various operating conditions. As shown in Fig. 6 and Fig. 7, for SVPWM and AZSPWM1 at low M_i the dominant harmonics are at twice the carrier frequency $2f_c$ (AZSPWM1 has some notable harmonics at f_c also). As shown in Fig. 8 and Fig. 9, DPWM1 dominant harmonics are at f_c. As shown in Fig. 10 and Fig. 11, NSPWM has harmonics both at f_c and $2f_c$. Depending on φ and M_i, the dominant term may become at f_c or $2f_c$. While $2f_c$ harmonic is dominant for φ = 0°, f_c harmonic is dominant for φ= 30º.

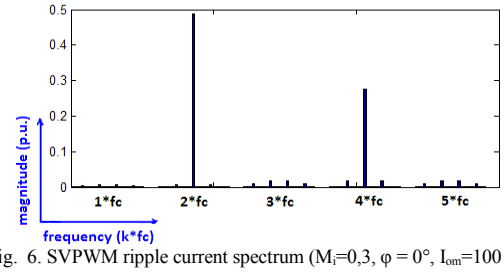

Fig. 6. SVPWM ripple current spectrum (M_i=0,3, φ = 0°, I_{om}=100 A)

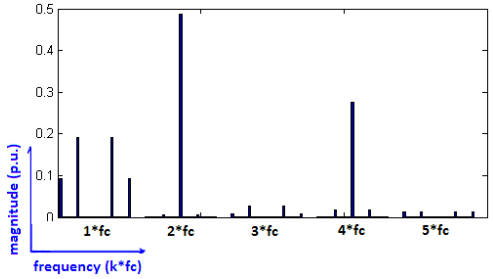

Fig. 7. AZSPWM1 ripple current spectrum (M_i=0,3, φ = 0°, I_{om}=100 A)

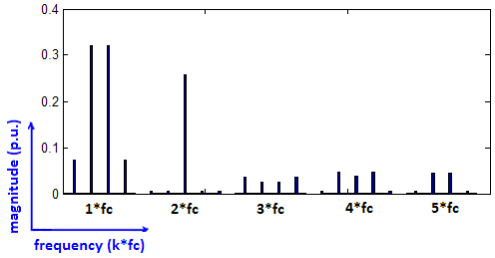

Fig. 8. DPWM1 ripple current spectrum (M_i=0,7, φ = 0°, I_{om}=100 A)

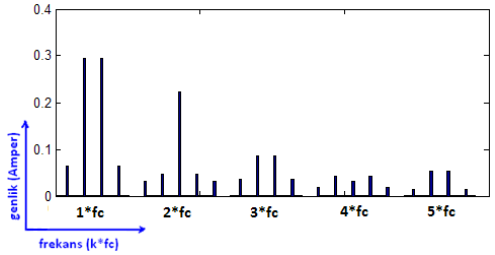

Fig. 9. DPWM1 ripple current spectrum (M_i=0,7, φ = 30°, I_{om}=100 A)

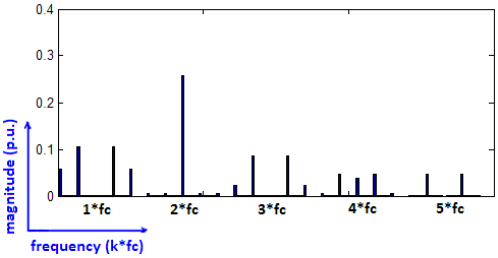

Fig. 10. NSPWM ripple current spectrum (M_i=0,7, φ = 0°, I_{om}=100 A)

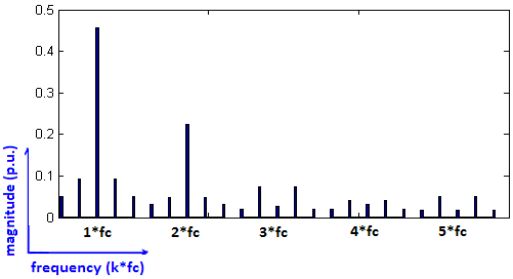

Fig. 11. NSPWM ripple current spectrum (M_i=0,7, φ = 30°, I_{om}=100 A)

C. Total RMS Value

In order to compare the DC link current ripple performance of the PWM methods, the ratio of the harmonic rms value of the DC link current $I_{h\text{-}rms}$ to the inverter AC output fundamental component current rms value I_{1rms} ($I_{om}/\sqrt{2}$) is evaluated and its square is termed as the DC link current coefficient K_{dc} [1]-[3] defined in (4).

$$K_{dc} = I^2{}_{h-rms} / I^2{}_{1rms} \tag{4}$$

For given M_i and φ, the RMS ripple DC link current is first calculated over a PWM cycle, then over a fundamental cycle to obtain $I_{h\text{-}rms}$. Then (4) is analytically calculated for all the methods discussed. Evaluating K_{dc} reveals some important attributes of the modulators. As Fig. 12 indicates, all methods are M_i and φ dependent. The reduced common mode voltage PWM methods have several times higher DC link current stress than the SVPWM and DPWM methods. At low M_i AZSPWM1 (especially at low cosφ) method exhibits large stresses. At higher cosφ the AZSPWM1 stresses become less. At higher M_i the DC link current stresses of the AZSPWM1 method become comparable to the conventional methods due to the expiration of the active zero state duration. The DC link current harmonic content of NSPWM is strongly dependent on PF and M_i. K_{dc} of NSPWM decreases with increasing M_i and PF. For PF=1, NSPWM has lower DC link ripple content than all other PWM methods. For PF of 0.8-0.9, K_{dc} of all PWM methods are similar. However, for PF lower than 0.6, K_{dc} of NSPWM is inferior to other methods.

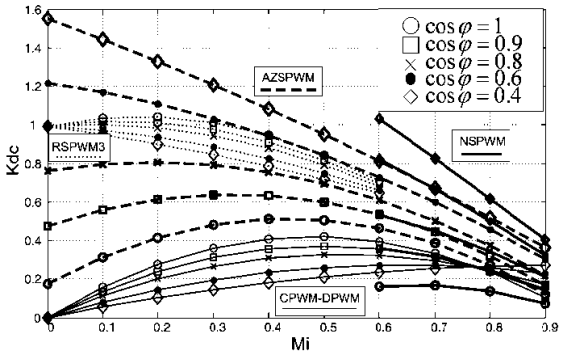

Fig. 12. RMS ripple current characteristics, K_{dc}=f(M_i,cosφ) for various PWM methods

IV. RIPPLE CURRENT SPECTRAL ANALYSIS

As apparent from the preceding section, the ripple current harmonic content is highly PWM method and operating point dependent. For inverter design and analysis purposes, it is necessary to have broad information on the spectra. Thus, a method to calculate the spectral content and a simple approach to be utilized in the inverter design is required. While detailed simulations are exhaustive and not intuitive, the simple rms value approach is insufficient. Thus in this section the double Fourier approach [4]-[6] will be utilized to obtain the spectral data, and in the next section a method to provide a simple design tool based on the data obtained from the double Fourier approach will be introduced.

The general analytical approach to obtain the exact harmonic content of periodically switching circuits involves the double Fourier approach. In this approach, first, the phase current waveforms and the PWM modulation waveforms are defined. Second, these functions are processed to obtain a raw F(x,y) function to be processed in the double integral. Finally, this process is executed via a numerical/symbolic double Fourier integral computational software. In terms of equations, using the integral of (5), the coefficients A_{mn} and B_{mn} are obtained, then the ripple current magnitude for each frequency is obtained as I_{mn} in (6). Here m corresponds to the carrier frequency and its multiples, and n corresponds to the fundamental component and its outputs. Thus, the

harmonics are at the $mf_c \pm nf_o$.As a result, the dc link current is obtained as the function F(x,y) given in (7). Of the four terms in (7), the first one gives the average current of (2). The second term gives the possible sub-carrier frequency components. The third term gives the carrier frequency and its multiples (center frequency harmonics). And the final term gives the sideband harmonics for the carrier and its multiples. The details of the double Fourier approach as applied to dc current ripple calculation are laid out in [6] and will not be further discussed in the paper.

$$A_{mn} + jB_{mn} = \frac{1}{2\pi^2} \cdot \int_0^{2\pi} \int_0^{2\pi} F(x,y) \cdot e^{j(mx+ny)} dxdy \qquad (5)$$

$$I_{mn} = \sqrt{A_{mn}^2 + B_{mn}^2} \qquad (6)$$

$$F(x,y) = \frac{A_{00}}{2} + \sum_{n=1}^{\infty} [A_{0n} \cdot \cos(ny) + B_{0n} \cdot \sin(ny)] + \sum_{m=1}^{\infty} [A_{m0} \cdot \cos(mx) + B_{m0} \cdot \sin(mx)] + \sum_{m=1}^{\infty} \sum_{n=\mp 1}^{\mp \infty} [A_{mn} \cdot \cos(mx+ny) + B_{mn} \cdot \sin(mx+ny)] \qquad (7)$$

Employing the above described double Fourier integral approach and utilizing advanced computational tools with double integral routines, the spectral components can be easily obtained. In this work, MATLAB software has been used for this purpose. The spectral data of Fig. 6 to Fig. 11 were obtained by this method. However, to confirm the results, detailed inverter simulation model was built via Simplorer power electronics simulation software and via FFT analysis of the dc link current the double Fourier results were verified.

While the double Fourier approach gives the spectral information, there are difficulties in applying this approach in practice. The approach involves advanced mathematical skills, and complex to implement for a typical design engineer. The spectral graphics are strongly dependent on the PWM method and operating conditions (M_i, φ, I_{om}). The wide range of harmonics are difficult to individually consider in the design. Thus simplification is necessary. The following section elaborates on this issue.

V. THE EQUIVALENT CENTERED HARMONIC APPROACH

Since the ripple current consists of carrier and sidebands and multiples with sidebands, it is difficult to evaluate the total effect of the ripple current by observing individual components (as there are too many terms). Using the total RMS value (as in Fig. 12) hides the frequency information, which is necessary in design and performance evaluation. Thus, an approach more informative than the rms value approach, but not as complicated as the full harmonic spectrum study is required.

As illustrated in Fig. 13, the equivalent centered harmonic approach developed in this paper lumps the ripple current carrier frequency component and its sidebands to the center (to the carrier frequency) as a single frequency equivalent. The same is done for the multiples of the carrier, for example harmonics at $2f_c$ and the sidebands are lumped at an equivalent harmonic at $2f_c$ and so on. The equivalent centered harmonic current equation for the m^{th} carrier multiple frequency $I_{h\text{-}me}$ is given in (8), where m is the multiple index of the carrier frequency and n is the sideband index. M and N define the range to be covered.

$$I_{h-me} = \sqrt{\sum_{n=-N}^{N} I_{h-mn}^2} \qquad m=1, ..., M \qquad (8)$$

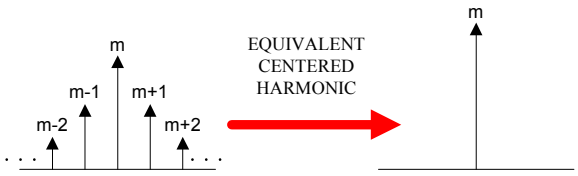

Fig. 13. The equivalent centered harmonic representing the carrier frequency harmonic and its sidebands

The equivalent harmonic concept has a physical meaning from the practical application perspective. In both electrolytic and film capacitors the loss mechanism involved is frequency dependent. In electrolytic capacitors the ESR and in the film capacitor the dielectric losses are frequency dependent. The carrier frequency and its sideband harmonics are typically very close to each other that in this range the losses don't vary significantly. Thus, in terms of losses the harmonics can be represented with one equivalent centered harmonic as defined in (8). In this case the equivalent harmonic approach may be used to calculate the losses with more accuracy than a simple rms or single frequency calculation. Similarly, in applications with small film capacitor, the voltage ripple can be approximately calculated based on the dominant equivalent harmonic term using the $V_{h\text{-}me}=I_{h\text{-}me}/(w_{me}C)$ terminal law.

In practice the dominant harmonics are in the first 4 terms and their sidebands (M=4). Thus, it is sufficient to consider harmonics from f_c to $4f_c$. In terms of sidebands, while a wide range can be considered, the first 10 (±10) are sufficient to represent the exact system (N=10). Considering this range, for the system parameters defined in section III.B, the equivalent centered harmonics have been calculated using equations (5) to (8) for the discussed PWM methods and a full range of M_i and PF was swept. Moreover, the ac output current has been normalized (100Apeak=1 unit) such that per unit equivalent harmonic content could be obtained. Using the MATLAB software, the formulas were executed and 3-D graphics were obtained as shown in Fig. 14. In the figure, the rms total value consistent with Fig. 12, and the first four equivalent centered harmonics (f_c, $2f_c$, $3f_c$, $4f_c$) are shown. Since it is given in normalized form, this graphic is general and can be used to obtain the harmonic information for any operating condition. Thus, a design engineer can use (look-up through the data) this graphic directly, and there is no more need for double Fourier analysis and detailed computer programming to do the calculations.

The 3-D graphic results show that for SPWM and SVPWM, the dominant harmonics are at m=2. For AZSPWM1, the first two harmonics are dominant (the $2f_c$ term being stronger), but the harmonics vary significantly and highly depend on the operating point. Thus, given an operating point the dominant harmonics could be selected by comparing all four harmonics. For DPWM1 the first two are dominant (the f_c term being stronger), and the rest should be taken into account depending on the operating point. For NSPWM, the operating point sensitivity is the strongest as the graphics show. Thus, given an operating point all the four components should be taken into consideration carefully. The results of Fig. 6 to Fig. 11 are consistent with the graphics and the results of this discussion. Furthermore, many additional simulations were conducted to verify the accuracy of the 3-D graphic data, and correlation was established. Thus only the 3-D graphic data is shown and simulation results omitted. As will be shown in the next section, based on the application type and its operating points, the selection of the right PWM method and later the inverter design in terms of dc bus capacitor sizing becomes possible by using these 3-D graphic results.

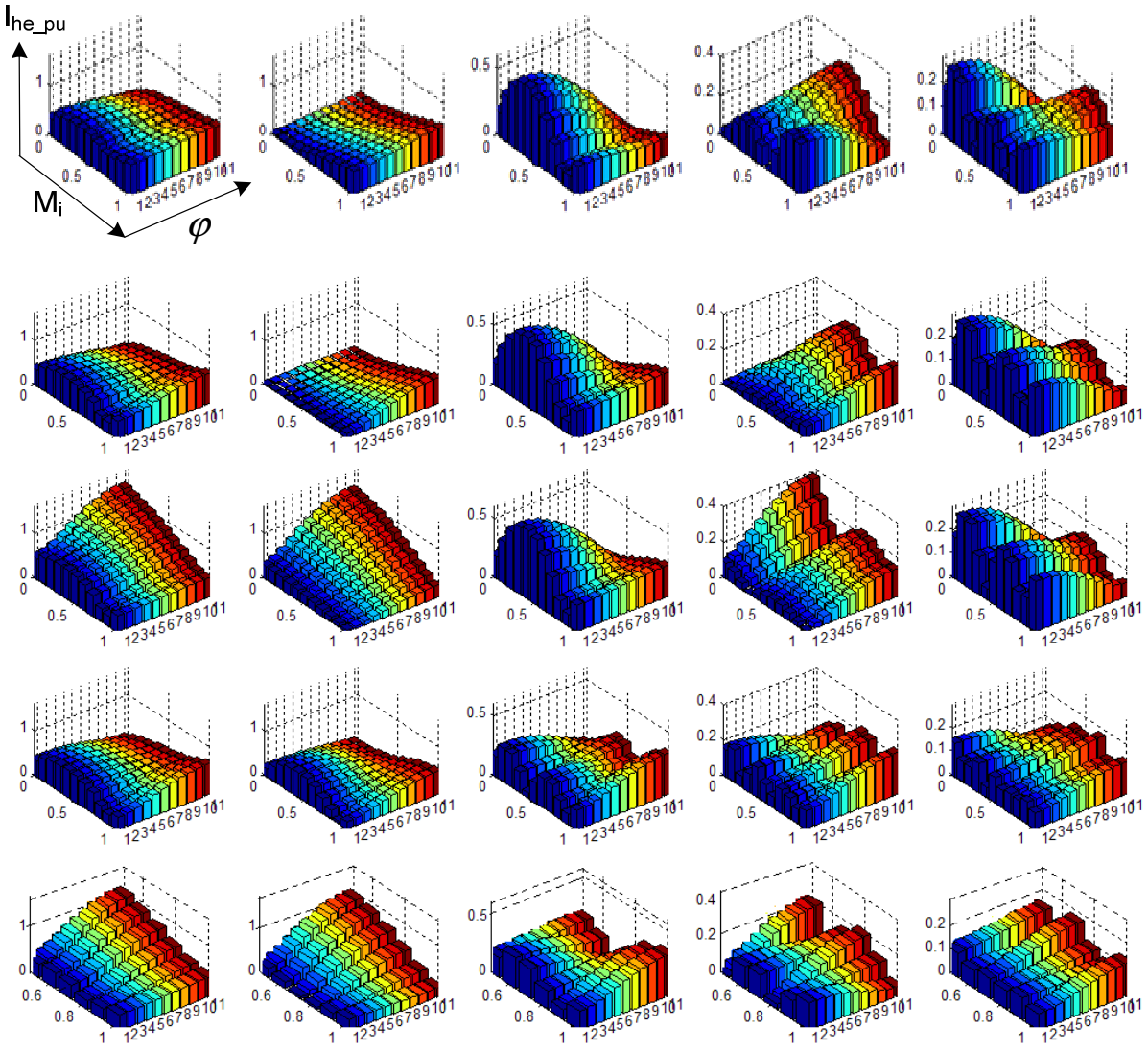

Fig. 14.The normalized rms and normalized equivalent centered dc bus current harmonics. From top to bottom: SPWM, SVPWM, AZSPWM1, DPWM1, NSPWM. From left to right: normalized rms value (scaled with √2), first centered harmonic peak value (m=1), second centered harmonic peak value (m=2), third centered harmonic peak value (m=3), fourth centered harmonic peak value (m=4).
M_i axis: 0 to 0.9 in 0.1 increments, and φ axis: 0º to 90º in 9° increments

VI. PWM METHOD SELECTION DEPENDING ON THE APPLICATION

Three-phase, two-level VSIs have three common applications. One is in driving ac motors/generators. The second involves grid interface, as PWM rectifier, uninterruptible power supplies (UPS) system grid side, renewable energy applications such as solar and wind power converters. The third application involves power supplies where sinusoidal output voltage is generated to feed passive/active loads (which can be considered similar to PWM rectifier application). In these applications, the typical operating points are summarized in Fig. 15.

Induction and servomotors while operating at low speed require low voltage corresponding to low M_i. Also both motors have near unity power factor steady-state behavior in this range. For induction machines high speed operation corresponds to lagging power factor and high M_i. For synchronous machines high speed operation typically corresponds to high M_i, but near unity power factor due to the field excitation or permanent magnet. For PWM rectifiers (used for AC/DC conversion, input of UPS systems) and renewable energy systems (PV, wind), operation against the power grid involves high M_i and typically the power factor is unity. DC/AC power supplies and UPS outputs also operate at single frequency and high M_i, but the load power factor is typically lagging and less than unity. In summary the operating points described in Fig. 15 cover most three-phase inverter applications.

For the selected operating points, assuming an ac load current with 100A (peak) per phase, and the parameters of section III.B, the dc bus ripple current rms value, the dominant equivalent harmonic components (termed as mD) have been evaluated and the results are comparatively listed in Table I for the four advanced PWM methods. SVPWM which is slightly inferior to SVPWM has not been included in the table. The results of the table are obtained from the 3-D graph of Fig. 14. In the table, I_{avg} is calculated from (2).

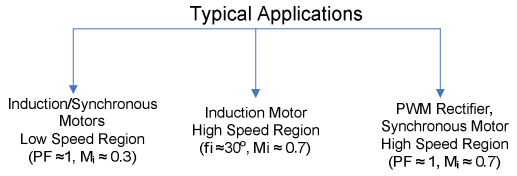

Fig. 15. PWM inverter applications and typical operating points

TABLE I. DC BUS RIPPLE CURRENT PERFORMANCE SUMMARY

PWM Method	$M_i = 0.3$ $\varphi = 0°$ I_{avg}=28,6 A		$M_i = 0.7$ $\varphi = 30°$ I_{avg}=58,1 A		$M_i = 0.7$ $\varphi = 0°$ I_{avg}=66,8 A	
	(I_{hf}) rms	mD	(I_{hf}) rms	mD	(I_{hf}) rms	mD
SVPWM	36,8	2	37,4	2	39	2
AZSPWM1	57,1	2	46,3	1,2	41,4	2
DPWM1	36,3	1	37,4	1	39,2	1
NSPWM	38,8	1,2	40,3	1	25,5	2

In terms of dc bus ripple current, for motor drive low speed applications SVPWM is the best method as it has the lowest rms ripple current and the dominant equivalent harmonic is at $2f_c$ (easy to filter). For induction motor drive at high speed AZSPWM1 is the worst method, while other methods exhibit some trade-off relations; SVPWM is the easiest to filter (with harmonics at $2f_c$), DPWM1 has low switching losses and similar rms ripple but more difficult to filter (with harmonics at f_c), NSPWM has low common mode voltage and similar rms ripple current characteristics to DPWM1. Thus, depending on the performance priorities set for the application, a method is chosen. For near unity PF and high M_i applications, as it appears clearly from the table, NSPWM is overall better method than all. This section, thus provides the first clear step in inverter dc bus side design by involving the PWM method choice. Having a PWM method selected, the next step involves the dc bus capacitor design. However, this step involves capacitor technology knowledge, which will be briefly summarized in the next section.

VII. REVIEW AND DESIGN OF DC BUS CAPACITORS FOR INVERTERS

Inverters with diode/thyristor rectifier inputs require large capacitors to filters to suppress the low frequency harmonics due to the input side. Thus, in such applications, electrolytic capacitors are the favorable choice, especially in voltage levels 500V or less. If the input involves a dc supply (such as battery, fuel cell, photovoltaic module) or a high frequency converter (dc-dc converter or, PWM rectifier), in this case, the filtering requirement is at high frequency and small capacitance is sufficient. In such cases film capacitors are favorable, and avaliable in a wide range expanding beyond 500V.

In electrolytic capacitors the component life and performance is highly temperature dependent. The ESR is the dominant loss mechanism, and it is frequency dependent. Especially in the sub kHz range the ESR is high and causes thermal problems if the ripple current is high. Typically not the voltage ripple criteria, but the current ripple criteria dominates the design. Film capacitors used in inverter applications have self-healing property, their thermal reliability is higher and their life is longer. Polyester and polypropylene capacitors are the most frequently used type. Dielectric losses are the dominant loss mechanism and the losses increase with frequency. Typically the voltage ripple criteria dominates the design. The reason that the film capacitor uses the voltage ripple criteria while the electrolytic capacitor uses the current ripple criteria is related to the ripple current capacity of these capacitor types. Film capacitor can carry 1A/μF, however, electrolytic capacitor can carry 20mA/μF [9]. In both electrolytic and film capacitor sizing for inverter application, alone with the capacitor manufacturer datasheet information, the ripple current information is necessary to estimate the losses and calculate the voltage ripple. Several papers and application notes elaborate on the design and performance issues of dc bus capacitors [7]-[13].

In the design, if the dominant ripple current (equivalent centered harmonic) is known, and the voltage ripple V_{ripple} is specified, then the required capacitance can be calculated as in (9). Given the C value, if the available capacitor has sufficient current ripple capability (to be checked through manufacturer datasheets), then this capacitor can be used. Otherwise, a capacitor with higher current capacity to accommodate the specified ripple current should be selected.

$$C = \frac{1}{2\pi \cdot f_{mD} \cdot V_{ripple}} \cdot I_{md} \quad (9)$$

VIII. DC BUS CAPACITOR DESIGN EXAMPLE

In this section, a renewable energy application (photovoltaic energy conversion system) will be considered. A three-phase 400V line-to-line-rms, 50Hz grid connection is considered. 50kW rating and unity power factor operation is assumed. PWM recitifer operation mode is valid. The dc bus ripple only comes from the rectifier side while the PV side is a smooth dc current source not causing ripple.

The design involves PWM rectifier operation (corresponding to $\varphi \approx 0^o$ and $M_i \approx 0.7$) with $V_{dc} = 800$ V, $I_{om} = 100$ A, and a switching frequency of 10 kHz. The most appropriate PWM method in the sense of minimum DC bus ripple current is NSPWM (25.5A in Table I). Based on the ripple current capacity discussion in section VII, in order to carry 25.5 A ripple current, 1275 µF electrolytic capacitor or 25.5 µF film capacitor is required. Typical commercial electrolytic capacitor can be choosen as 4.1 mF 400 V dc with ESR of 33mΩ @ 10kHz and dimensions D = 76.2 mm x L = 130.2 mm with maximum I_{rms} = 45 A at T_{amb} = 50 °C. Moreover, two of these electrolytics must be connected in series to form 800 volts dc bus. On the other hand, typical commercial film capacitor parameters are 90µF 900 V with ESR of 5 mΩ @ 10kHz and dimensions D = 80.2 mm x L = 76.8 mm with maximum I_{rms} of 42 A at T_{amb} = 50 ºC. Therefore, 1.18 liters of electrolytic capacitor is used while 0,39 liters of film capacitor is used for same application. Hence, much smaller size and longer life with film capacitor.

The power dissipation of electrolytic capacitor can be found from $P_{diss} = I_{rms}^2 \cdot R_{ESR}$ and the power dissipation of film capacitors can be found from $P_{diss} = I_{rms\_f}^2 \cdot R_{ESR\_f} + \frac{1}{2} \cdot C_n \cdot V_{peak\ to\ peak}^2 \cdot f$. Therefore, the loss for series electrolytic capacitors can be calculated as $P_{diss} = 2 \cdot 25.5^2 \cdot 0.033 = 43\,W$. Moreover, with $I_{md} = 20A$ from Fig. 14 and I_{md} is at $2f_c$, the loss for film capacitor can be calculated as $P_{diss} = 25.5^2 \cdot 0{,}005 + 0{,}5 \cdot 90 \cdot 10^{-6} \cdot \left(\frac{1}{5{,}65} \cdot 20\right)^2 \cdot 20000 = 3{,}25 + 11{,}3 = 14.6\,W$.

IX. CONCLUSION

This paper reviewed the dc bus ripple current characteristics of three-phase voltage source inverters, evaluated the spectral characteristics, and provided a simple approximation for spectral components. The equivalent centered harmonic approach models the carrier and sideband dc bus capacitor current harmonics with an equivalent harmonic at the center (same is applied to the multiples of f_c). This simplification aids in clear understanding the dominant harmonics and their effects. As a consequence, with this approach, capacitor losses (ESR or dielectric) and voltage ripple can be accurately calculated. The centered current harmonics are put in 3-D graphic for look-up to be used in dc bus capacitor design. Therefore, the designer does not have to do complex calculations such as double Fourier integrals and involved computational algorithms. In the paper, design rules are established and a design example is given. The paper additionally evaluates and suggests PWM methods for various inverter applications with the dc bus ripple performance being the main constraint. With the help of the study in this paper, a better inverter and dc bus capacitor design can be achieved.

REFERENCES

[1] P. A. Dahono, Y. Sato, T. Kataoka, "Analysis and minimization of ripple components of input current and voltage of PWM Inverters," Conf. Rec. IEEE IAS Annu. Meeting, 1995, pp. 2444–2450.

[2] A. M. Hava, R. J. Kerkman, and T. A. Lipo, "Simple analytical and graphical methods for carrier-based PWM-VSI drives," IEEE Trans. Power Electron., vol. 14, no. 1, pp. 49–61, Jan. 1999.

[3] A. M. Hava and E. Ün, "Performance analysis of reduced common-mode voltage PWM methods and comparison with standard PWM methods for three-phase voltage source inverters," IEEE Trans. Power Electron., vol. 24, no. 1, pp. 241–252, Jan. 2009.

[4] H. Zhang, N. Wheeler, D. Grant, "Switching harmonics in the DC link current in a PWM AC-DC-AC converter," Conf. Rec. IEEE IAS Annu. Meeting, 1995, pp. 2649–2655.

[5] P.B. McGrath, D.G. Holmes, "A general analytical method for calculating inverter dc-link current harmonics," IEEE Trans. Ind. Applicat., vol. 45, No.5, pp. 1851-1859. Sept./Oct., 2009.

[6] M. H. Bierhoff, M. W. Fuchs," DC-link harmonics of three-phase voltage source converters influenced by the pulsedwidth-modulation strategy-an analysis", IEEE Trans. Power Electron., vol. 55, no. 5, May 2008, pp. 2085–2092.

[7] S.G. Parler, Jr., P.E., "Deriving life multipliers for electrolytic capacitors," IEEE Power Electronics Society Newsletter, vol. 16, no. 1, pp. 11-12, Feb. 2004.

[8] "c04-appguide" Cornell Dubilier.

[9] G. Terzulli, "Film technology to replace electrolytic technology in wind power applications," TPC, division of AVX Corporation.

[10] http://www.windpowerengineering.com/maintenance/safety/films-in-capacitors-let-them-self-heal-and-more/

[11] Kemet ALS42 Series Datasheet.

[12] "AVX Medium Power Film Capacitors for Power Applications," AVX Corporation.

[13] "DC Film Capacitors", Cornell Dubilier.

[14] R.M. Tallam, R.J. Kerkman, D. Leggate and R.A. Lukaszewski, "Common-mode voltage reduction PWM algorithm for AC drives," IEEE Trans. Ind. Applicat., vol. 46, no. 5, pp. 1959-1969. Sep./Oct. 2010.

[15] E. Ün, A.M. Hava "A near state PWM method with reduced switching frequency and reduced common mode voltage for three-phase voltage source inverters," IEEE Trans. Ind. Applicat., vol. 45, No.2, pp. 782-793. Mar./Apr. 2009.

[16] A.M. Hava and N.O. Çetin, "Scalar PWM approach with easy implementation features for three-phase, three-wire voltage source inverters," IEEE Transactions on Power Electronics, Vol.26, no. 5, pp. 13851-1395, May 2011.